Biochimica et Biophysica Acta 1818 (2012) 1706–1716

Contents lists available at SciVerse ScienceDirect

Biochimica et Biophysica Acta

journal homepage: www.elsevier.com/locate/bbamem

Flexibility of the PDZ-binding motif in the micelle-bound form of Jagged-1 cytoplasmic tail

Matija Popovic [a], Ventsislav Zlatev [a], Vesna Hodnik [b], Gregor Anderluh [b,c], Isabella C. Felli [d], Sándor Pongor [a,*], Alessandro Pintar [a,*]

[a] Protein Structure and Bioinformatics Group, International Centre for Genetic Engineering and Biotechnology (ICGEB), AREA Science Park, Padriciano 99, I-34149 Trieste, Italy
[b] Department of Biology, Biotechnical Faculty, University of Ljubljana, Večna pot 111, 1000 Ljubljana, Slovenia
[c] Laboratory for Biosynthesis and Biotransformation, National Institute of Chemistry, Hajdrihova 19, 1000 Ljubljana, Slovenia
[d] Magnetic Resonance Center and Department of Chemistry, University of Florence, Via Luigi Sacconi 6, I-50019 Sesto Fiorentino, Italy

ARTICLE INFO

Article history:
Received 9 November 2011
Received in revised form 13 March 2012
Accepted 14 March 2012
Available online 21 March 2012

Keywords:
Notch signaling
Membrane/cytoplasm interface
Phosphorylation
NMR
Surface plasmon resonance
Circular dichroism

ABSTRACT

Human Jagged-1, one of the ligands of Notch receptors, is a transmembrane protein composed of a large extracellular region and a 125-residue cytoplasmic tail which bears a C-terminal PDZ recognition motif. To investigate the interaction between Jagged-1 cytoplasmic tail and the inner leaflet of the plasma membrane we determined, by solution NMR, the secondary structure and dynamics of the recombinant protein corresponding to the intracellular region of Jagged-1, J1_tmic, bound to negatively charged lysophospholipid micelles. NMR showed that the PDZ binding motif is preceded by four α-helical segments and that, despite the extensive interaction between J1_tmic and the micelle, the PDZ binding motif remains highly flexible. Binding of J1_tmic to negatively charged, but not to zwitterionic vesicles, was confirmed by surface plasmon resonance. To study the PDZ binding region in more detail, we prepared a peptide corresponding to the last 24 residues of Jagged-1, J1C24, and different phosphorylated variants of it. J1C24 displays a marked helical propensity and undergoes a coil–helix transition in the presence of negatively charged, but not zwitterionic, lysophospholipid micelles. Phosphorylation at different positions drastically decreases the helical propensity of the peptides and abolishes the coil–helix transition triggered by lysophospholipid micelles. We propose that phosphorylation of residues upstream of the PDZ binding motif may shift the equilibrium from an ordered, membrane-bound, interfacial form of Jagged-1 C-terminal region to a more disordered form with an increased accessibility of the PDZ recognition motif, thus playing an indirect role in the interaction between Jagged-1 and the PDZ-containing target protein.

1. Introduction

Ligands to Notch receptors are type I membrane spanning proteins. They all share a poorly characterized N-terminal region, a DSL (Delta/Serrate/Lag-2) domain, a series of tandem epidermal growth factor-like repeats, a transmembrane segment, and a unique cytoplasmic tail of ~100–150 amino acids [1]. Five different ligands to Notch receptors have been identified in mammals, three orthologs (Delta-1, -3 and -4) of *Drosophila* Delta and two orthologs (Jagged-1 and -2) of *Drosophila* Serrate. Although the molecular mechanisms of ligand specificity are still unclear, evidence from *in vivo* studies suggests that each ligand exerts non-redundant effects. Gene knock-out of Jagged-1 [2] or Delta-1 [3], heterozygous deletion of Delta-4 [4], or homozygous mutants in Jagged-2 [5] all lead to severe developmental defects and embryonic lethality in mice. There is no significant sequence similarity shared among the intracellular region of the different ligands [6], apart from the identical PDZ binding motif (ATEV) found at the C-terminus of Delta-1 and Delta-4. Neither Delta-3 nor Jagged-2 presents a PDZ recognition motif whereas the cytoplasmic tail of Jagged-1 contains a different C-terminal PDZ interacting motif (EYIV). Jagged-1 was shown indeed to interact in a PDZ-dependent manner with afadin (AF6), a protein located at cell–cell adherens junctions [7,8]. The cytoplasmic tail of Notch ligands is also a target for ubiquitination and ligand endocytosis. Both Mind bomb 1 [9–11] and a myrystoylated, membrane-anchored form of Neuralized-like 1 [12] have been proposed to be involved in

Abbreviations: DMPC, 1,2-dimyristoyl-*sn*-glycero-3-phosphocholine; DMPG, 1,2-dimyristoyl-*sn*-glycero-3-[phospho-*rac*-(1-glycerol)] sodium salt; DMPS, 1,2-dimyristoyl-sn-glycero-3-[phospho-L-serine] sodium salt; DSS, 2,2-dimethyl-2-silapentane-5-sulfonate-d_6 sodium salt; HSQC, heteronuclear single quantum correlation; LMPC, 1-myristoyl-2-hydroxy-*sn*-glycero-3-phosphocholine; LMPG, 1-myristoyl-2-hydroxy-*sn*-glycero-3-[phospho-*rac*-(1-glycerol)] sodium salt; LPPC, 1-palmitoyl-2-hydroxy-*sn*-glycero-3-phosphocholine; LPPG, 1-palmitoyl-2-hydroxy-*sn*-glycero-3-[phospho-*rac*-(1-glycerol)] sodium salt; PDZ, domain present in PSD-95, Dlg, and ZO-1/2; POPG, 1-palmitoyl-2-oleoyl-*sn*-glycero-3-phospho-(1′-*rac*-glycerol) sodium salt; SDS, sodium dodecyl sulfate; SPR, surface plasmon resonance; TFE, 2,2,2-Trifluoroethanol

* Corresponding authors. Tel.: +39 040 3757354; fax: +39 040 226555.
E-mail addresses: pongor@icgeb.org (S. Pongor), pintar@icgeb.org (A. Pintar).

0005-2736/$ – see front matter © 2012 Elsevier B.V. All rights reserved.
doi:10.1016/j.bbamem.2012.03.012

mono-ubiquitinylation of Jagged-1 in mice. Finally, there is compelling evidence that Notch ligands, much alike Notch receptors, undergo ectodomain shedding and regulated intramembrane proteolysis. The proteolytic processing of Jagged-1 is mediated by the ADAM17 metalloprotease [13,14] and by the presenilin/γ-secretase complex [13]. Although the fate of the cleaved intracellular region is still unclear, it is possible that it acts as a membrane-tethered transcriptional co-activator. The C-terminal fragment of Jagged-1 comprising part of the transmembrane segment and the intracellular region expressed in COS cells was shown to localize mainly in the nucleus, and to activate gene expression through the transcription factor activator protein 1 (AP1/p39/*jun*) enhancer element [13].

Depending on the environment, the intracellular region of Jagged-1 is then supposed to exist in at least two distinct forms, as a membrane-tethered protein located at the interface between the membrane and the cytoplasm and as a soluble nucleocytoplasmic protein. In a previous study [15], we showed that a recombinant protein corresponding to the cytoplasmic tail of human Jagged-1 (J1_tmic) is mainly disordered in solution, but has a distinct propensity to adopt a helical conformation in the presence of TFE. J1_tmic also gains secondary structure upon binding to the negatively charged surface of SDS micelles, or to vesicles made of negatively charged phospholipids such as DMPS and DMPG, which are prevalent components of the inner layer of the plasma membrane in eukaryots. On the contrary, the structure of J1_tmic is not affected by the presence of vesicles formed by a zwitterionic phospholipid like DMPC, suggesting that the negative charge density at the surface of SDS micelles or lipid vesicles is required to promote binding and secondary structure formation. We also showed that helix formation is strongly pH-dependent, with a sharp increase in the helical content from pH ~7 to ~6. As J1_tmic contains six endogenous histidines, we suggested that protonation of one or more of the histidines is promoting helix formation or extension.

The partial folding of the cytoplasmic domain of Jagged-1 accompanied by its association with the inner side of the cell membrane may have relevant effects on the function of Jagged-1 in Notch signaling. For instance, it would selectively mask certain residues that are potential targets for post-translational modifications such as phosphorylation, ubiquitinylation, or O-glycosylation with β-N-acetylglucosamine. In a similar way, it would mask or expose selected binding motifs with respect to binding partners. The partial folding and association of the intracellular region of Jagged-1 with the membrane is also expected to reduce the accessibility of the PDZ binding motif. To get more insight into the interaction between Jagged-1 cytoplasmic tail and the membrane, we studied a model system made of the recombinant protein corresponding to the cytoplasmic tail of Jagged-1 (J1_tmic) and negatively charged lysophospholipid micelles used to mimic the interface between the plasma membrane and the cytosol. We applied solution NMR methods to determine the secondary structure and dynamics of J1_tmic bound to micelles. Furthermore, we hypothesized that phosphorylation of selected residues close to the PDZ binding motif might alter the affinity for the negatively charged inner layer of the cytoplasmic membrane and possibly change the conformational properties of Jagged-1 C-terminal region. To test this hypothesis, a series of peptides corresponding to the C-terminal sequence of Jagged-1 (JAG1_HUMAN, residues 1195–1218) and phosphorylated at different positions was synthesized, and their conformational properties studied by far-UV circular dichroism.

2. Materials and methods

2.1. Protein expression and purification

The recombinant protein corresponding to the cytoplasmic tail of human Jagged-1, starting from the putative presenilin/γ-secretase cleavage site and with the transmembrane cysteine mutated to alanine (residues 1086–1218 of JAG1_HUMAN; C1092A; see Supporting Material, Fig. S1) was expressed in BL21(DE3) *Escherichia coli* (Novagen) cells from a codon-optimized synthetic gene and purified in two steps by immobilized metal ion affinity chromatography followed by RP-HPLC, as described [15]. For the preparation of the ^{15}N- and of the ^{15}N, ^{13}C-labeled proteins, cells were grown in a minimal medium containing 6 g/L Na_2HPO_4, 3 g/L KH_2PO_4, 0.5 g/L NaCl, 0.12 g/L $MgSO_4$, 0.01 g/L $CaCl_2$, 1.7 g/L yeast nitrogen base without amino acids and ammonium sulfate (Difco), and 100 μg/mL ampicillin, supplemented with 0.5 g/L $^{15}NH_4Cl$, 5 g/L D-glucose or 0.5 g/L $^{15}NH_4Cl$, 5 g/L U-$^{13}C_6$ D-glucose for the single and doubly labelled proteins, respectively. Expression and purification of the labelled proteins were carried out as described above. The purified proteins were analyzed by LC–MS to confirm their identity.

2.2. NMR sample preparation

The protein stock solutions were prepared dissolving the freeze-dried labeled proteins in sodium phosphate buffer (20 mM), pH 6.1. Lysophospholipid stock solutions were prepared dissolving the 1-Myristoyl-2-Hydroxy-*sn*-Glycero-3-[phospho-*rac*-(1-glycerol)] sodium salt (LMPG) or 1-Myristoyl-2-Hydroxy-*sn*-Glycero-3-Phosphocholine (LMPC) (Avanti Polar Lipids Inc., Alabaster, AL, USA) in sodium phosphate buffer (20 mM, pH 6.1). The mixed micelle (LMPC/LMPG, 80/20 mol/mol) lysophospholipid stock solution was prepared dissolving the lysophospholipids in $CH_3OH/CHCl_3$, mixing the appropriate volumes of the two, gently drying the solution, and redissolving the mixture in sodium phosphate buffer, pH 6.1. Samples for NMR spectroscopy were prepared mixing the appropriate volumes of stock solutions, and adding D_2O (10 vol.%).

The final protein concentration was ~0.1 mM for the reference sample dissolved in buffer only, ~0.5 mM for the ^{15}N-labeled samples in the presence of LMPG (80 mM), LMPC (80 mM) or LMPC/LMPG (80 mM), and 0.9 mM for the ^{15}N, ^{13}C-labeled protein in the presence of LMPG (150 mM). Assuming a micelle aggregation number of ~120, the protein/micelle molar ratio was ~0.75. An additional sample with a protein concentration of ~0.33 mM and a LMPC/LMPG (80/20 mol/mol) concentration of 113 mM, which corresponds to a protein/micelle ratio of 0.35 was also prepared. From an average micelle aggregation number of ~120, a MW of 478.5 for each LMPG molecule, and a 1:1 stoichiometry, the calculated MW of the complex would be ~73 kDa.

2.3. NMR spectroscopy

NMR data were acquired at 298 K. Preliminary and ^{15}N relaxation experiments were acquired on a Bruker Avance 500 MHz spectrometer equipped with a TXI triple resonance cryoprobe using the ^{15}N-labeled protein. For assignment purposes, standard HNCACB, CBCA(CO)NH, HNCACO, HNCO and HN(CA)NNH experiments were acquired on Bruker Avance 700 and 800 MHz spectrometers equipped with cryogenic probeheads optimized for ^{1}H detection. The protonless experiments CON, (H)CBCACON and (H)CBCANCO [16–18] were acquired on a Bruker Avance 700 MHz equipped with a cryogenic probehead optimized for ^{13}C direct detection. $^{3}J_{HNH\alpha}$ coupling constants and exchange rates of backbone amides with solvent were estimated from HNHA [19] and CLEANEX-PM [20] experiments, respectively. Data were processed using XwinNMR and analyzed with the CCPN program ANALYSIS (http://www.ccpn.ac.uk). Chemical shifts were referenced to DSS. Deviations of Cα, C′, Hα, and Cβ chemical shifts from random coil values [21] were used to determine secondary structure regions. R_1 and R_2 relaxation rates were estimated from fitting a three parameter exponential decay to experimental intensities of HN cross peaks acquired with delays of 0.010, 0.150, 0.540, 1.00, 2.50 s for R_1 and 17, 68, 153, 204, 271 ms for R_2 experiments. ^{1}H–^{15}N steady-state

heteronuclear NOEs were obtained from the ratio of peak heights in paired spectra collected with and without proton saturation during the relaxation delay. $^{3}J_{HNH\alpha}$ coupling constants were calculated from the intensity ratio between the Hα cross peak and the diagonal HN peak using the formula $I_{H\alpha}/I_{HN} = -\tan^2(2\cdot\pi\cdot J\cdot\xi)$ where J is the $^{3}J_{HNH\alpha}$ coupling constant and $\xi = 13.05$ ms. No correction for relaxation effects was applied. Solvent-HN exchange rates were estimated plotting peak intensity ratios of HN cross peaks in the CLEANEX-PM and the reference HSQC spectrum vs. mixing times (10, 20, 30, 40 and 60 ms) and fitting the signal increase with a three parameter exponential. Exchange rates were also estimated from the intensity ratio between the exchange cross peak at the solvent resonance frequency and the HN diagonal peak in the ^{15}N-edited 3D NOESY-HSQC experiment.

2.4. Peptide synthesis. Peptides corresponding to Jagged-1 C-terminal region

(J1C24: Ac-NWTNKQDNRDLESAQSLNRMEYIV-COOH; J1C24RQ: Ac-NWTNKQDNRDLESAQSLNQMEYIV-COOH; J1C24pY: Ac-NWTNKQDNRDLESAQSLNRMEpYIV-COOH; J1C24pS: Ac-NWTNKQDNRDLESAQpSLNRMEYIV-COOH; J1C24pSpY: Ac-NWTNKQDNRDLESAQpSLNRMEpYIV-COOH; J1C24pTpS: Ac-NWpTNKQDNRDLEpSAQSLNRMEYIV-COOH; pS, phosphoserine; pT, phosphothreonine; pY, phosphotyrosine) were prepared by standard solid-phase Fmoc methods, as described [22]. Briefly, peptides were synthesized on a NovaSyn TGT (Novabiochem) resin using a home-built automatic synthesizer based on a Gilson Aspec XL SPE, acetylated at the amino-terminal group with 20% Ac_2O, and the peptide-resin cleaved/deprotected. Crude peptides were purified by semi-preparative RP-HPLC on a Zorbax 300SB-C18 column (9.4×250 mm, 5 μm, Agilent) and freeze-dried. The identity of the peptides was checked by LC–MS and the purity (>95%) estimated from RP-HPLC.

2.5. Circular dichroism

Samples for CD spectroscopy were prepared dissolving the freeze-dried J1_tmic protein or the J1C24 peptides in 5 mM Tris/HCl buffer, pH 7.4, to obtain stock solutions that were further diluted appropriately. Concentrations were estimated from the UV absorbance at 280 nm using the calculated extinction coefficients (16500 $M^{-1}\,cm^{-1}$ and 6990 $M^{-1}\,cm^{-1}$ for J1_tmic and the J1C24 peptides, respectively). Far-UV CD spectra were recorded for J1_tmic (7.5 μM) and for the J1C24 peptides (~40 μM) in buffer alone, in the presence of different concentrations of TFE, and in the presence of 1 mM (for J1_tmic) or 3 mM (for the J1C24 peptides) LMPG or LMPC at 25°C on a Jasco J-810 spectropolarimeter (JASCO International Co., Tokyo, Japan) using 1 mm pathlength quartz cuvettes. Additional spectra were acquired after adjustment of the pH to 6.0 through addition of small aliquots of 0.1 N HCl. Typically, five scans were acquired in the 190–250 nm range for each spectrum, at a scan rate of 20 nm min^{-1}. Mean residue ellipticity (MRE = deg cm^2 $dmol^{-1}$ $residue^{-1}$) was calculated from the baseline-corrected spectrum. A quantitative estimation of secondary structure content was carried out by deconvolution of far-UV CD spectra using the DichroWeb server (www.cryst.bbk.ac.uk/cdweb/html/home/html). Helical content was also estimated from the mean residue ellipticity at 222 nm according to the formula $[\alpha] = -100\cdot MRE_{222}/40000\cdot(1-2.57/N)$, where N is the number of peptide bonds.

2.6. Surface plasmon resonance

DMPG or DMPC in chloroform was dried under reduced pressure in round-bottom flasks to obtain a lipid film. The lipids were hydrated in 10 mM Hepes, 150 mM NaCl, pH 7.4 to form multilamellar vesicles. The large unilamellar vesicles were then prepared by extrusion of multilamellar liposome suspension through polycarbonate filters with 100 nm pore size. The vesicles were diluted 10 times for DMPG and 40 times for DMPC prior the capturing onto the chip in the running buffer (10 mM Hepes, 150 mM NaCl; the experiments were performed at pH 6.0 and 7.4).

The surface plasmon resonance (SPR) measurements were performed using Series S sensor chips L1 (Biacore, GE Healthcare) and the optical sensor Biacore T100 (Biacore, GE Healthcare) [23,24]. The system was primed twice with the running buffer and the chip was conditioned using 4 startup cycles. The vesicles were deposited at a low flow rate (2 μL/min) for 60 s for DMPG and 90 s for DMPC to reach the similar immobilization level (3500–4000 response units). After the capturing, the buffer was allowed to run 300 s over the surface to stabilize the vesicles on the chip. Then the samples were injected for 180 s and the dissociation was monitored for additional 180 s. The dilutions were prepared dissolving the freeze-dried J1_tmic in the running buffer and the concentrations used to monitor the binding of J1_tmic to DMPG were 0.195, 0.39, 0.78, 1.56, 3.13, 6.25, 12.5 and 25 μM. The surface was regenerated using two 30 s injections of 40 mM octyl β-D-glucopyranoside and one 12 s injection of 0.05% sodium dodecyl sulfate (SDS). The sample and regeneration solutions were injected at flow rate 10 μL/min. All experiments were performed at 25 °C. The binding responses were evaluated with the T100 Evaluation Software. Dissociation constants (K_d) were estimated from the equilibrium binding levels 4 s before the stop of the injection. The responses were fitted to the Steady State Affinity model. K_ds were obtained from two independent titrations.

3. Results

3.1. Secondary structure and dynamics of J1_tmic bound to lysophospholipid micelles

Far-UV CD spectra of J1_tmic in buffer at neutral pH is typical of disordered proteins, with a minimum at 200 nm and ellipticity close to zero at 190 nm (Fig. 1). While the far-UV CD spectrum remains unchanged in the presence of zwitterionic LMPC micelles, the minimum shifts at 204 nm and the ellipticity at 190 nm becomes positive when J1_tmic is dissolved in the presence of negatively charged LMPG micelles (Fig. 1). At pH 6.0, the negative band is further shifted

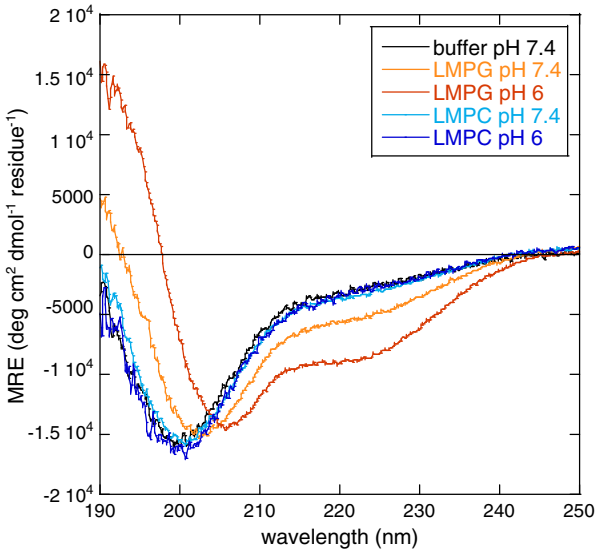

Fig. 1. Circular dichroism of J1_tmic. Far-UV CD spectra of J1_tmic (7.5 μM) in 5 mM Tris·HCl buffer, and in the presence of 1 mM lysophospholipids (LMPC or LMPG) at pH 7.4 or pH 6.0.

at 208 nm, and the shoulder at 222 nm as well as the positive band at 190 nm become more evident. These changes suggest a transition from a mainly disordered state to a partially folded, helical conformation of J1_tmic in the presence of LMPG but not LMPC micelles and confirm secondary structure predictions (Supporting Material, Fig. S1) and the helical propensity of J1_tmic previously observed in the presence of TFE, SDS micelles, and DMPG liposomes [15]. The helical content estimated from deconvolution of CD spectra is ~20% for J1_tmic in the presence of LMPG micelles at neutral pH, and increases to ~30% at pH 6 (Supporting Material, Table S2).

In agreement with CD results, SPR measurements showed that the binding of J1_tmic to chip-immobilized DMPG liposomes was concentration dependant and stable at pH 6.0 or 7.4 (Fig. 2). The estimated K_d for J1_tmic binding to lipid vesicles was evaluated to be 0.9 ± 0.14 and 3.5 ± 0.7 μM for pH 6.0 and 7.4, respectively. J1_tmic did not bind to DMPC vesicles at 25 μM, the highest used concentration, at any pH (Fig. 2).

To map the helical segments onto the sequence, we used heteronuclear solution NMR techniques. From preliminary NMR spectra of J1_tmic dissolved in buffer, 115 backbone NH cross-peaks (~92% of the total) of the 125 expected could be detected in the HSQC spectrum, including those arising from the three glycines (Supporting Material, Fig. S2). The amide resonances display very limited chemical shift dispersion in the ^{1}H dimension (7.6–8.7 ppm), and several residues seem to have a major and a minor form. In the 7.2–7.3 ppm range in the ^{1}H dimension (~125 ppm in the folded ^{15}N dimension), three peaks tentatively assigned to the $^{\varepsilon}$NH of the R side chains are detectable, two of which are broad and overlapped. The $^{\varepsilon 1}$NH peaks of the two W side chains appear as distinct resonances, although very close in chemical shift (10.09 and 10.11 ppm). The amide resonances of the 21 N/Q side chains are all clustered in a narrow region.

The HSQC spectrum of ^{15}N-J1_tmic in the presence of LMPC micelles (Supporting Material, Fig. S2) is very similar to that in buffer, with no or very little chemical shift variation for most of the resonances. The only significant differences are the doubling of W side chain $^{\varepsilon 1}$NHs with two new peaks at 10.30 and 10.35 ppm, suggesting the presence of a major and a minor form (Supporting Material, Fig. S3) and the appearance of three peaks in the 7.5–7.7 ppm range (7.51/118.76; 7.58/117.28; 7.71/118.27).

On the contrary, the HSQC spectrum of ^{15}N-J1_tmic in the presence of LMPG micelles (Fig. 3) is significantly different, with 119 detectable peaks, including those arising from the three glycines (~95% of the total), a new set of resonances appearing in the 7.5–7.8/116.3–118.5 (^{1}H/^{15}N) ppm region and a set of at least six distinct peaks possibly arising from the $^{\varepsilon}$NH of the arginine side chains. The amide resonances of the N/Q side chains show a larger chemical shift dispersion and many of them appear as distinct pairs of peaks. Increasing the temperature from 298 K to 308 K, or decreasing it to 288 K did not improve the appearance of the HSQC spectrum in a significant way.

The spectrum of ^{15}N-J1_tmic in the presence of mixed LMPC/LMPG micelles seems to be intermediate between the two spectra recorded in the presence of either LMPC or LMPG micelles, and decreasing the protein/lipid ratio did not yield significant changes.

Sequential assignments of the backbone were achieved using standard triple resonance spectra, supported by NOESY and "protonless" experiments. Assignments in the N-terminal half were particularly difficult because of the line broadening and low intensity – sometimes under detection limits – of HN resonances in the ^{1}H–^{15}N HSQC spectrum. Assignments of the C-terminal half residues, including the presence of five prolines, were more straightforward due to sharper HN cross-peaks, especially in the last 10–20 residues that

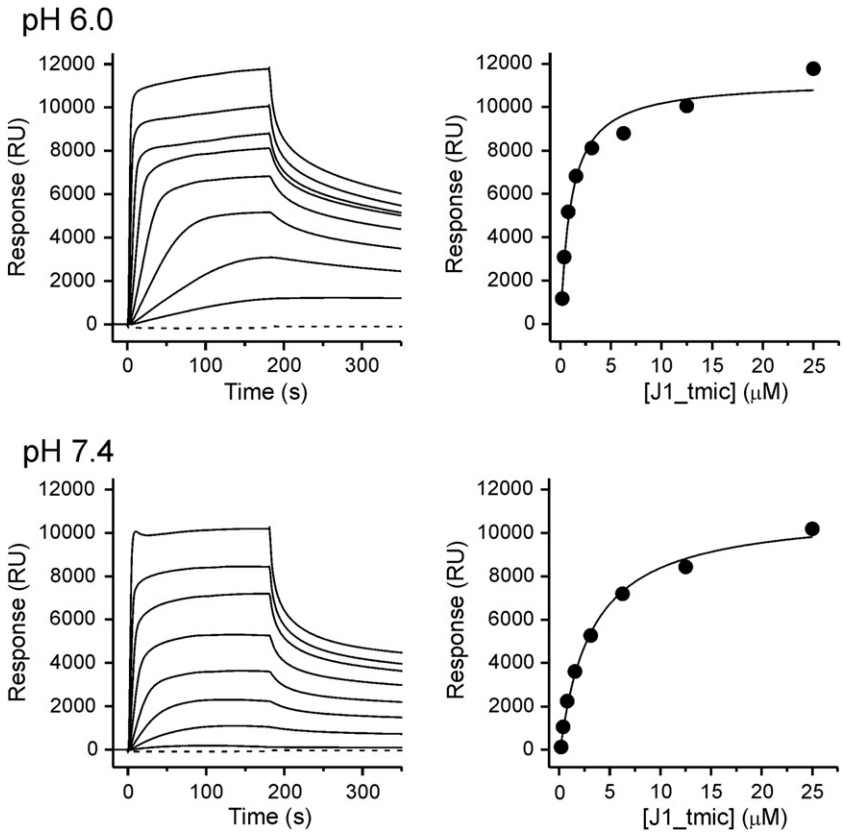

Fig. 2. Surface plasmon resonance. Binding of J1_tmic to large unilamellar vesicles as measured by SPR. Black thin lines, binding to DMPG liposomes. Concentrations used were 0.195, 0.39, 0.78, 1.56, 3.13, 6.25, 12.5 and 25 μM from bottom to top. Dashed line, binding of 25 μM J1_tmic to DMPC liposomes.

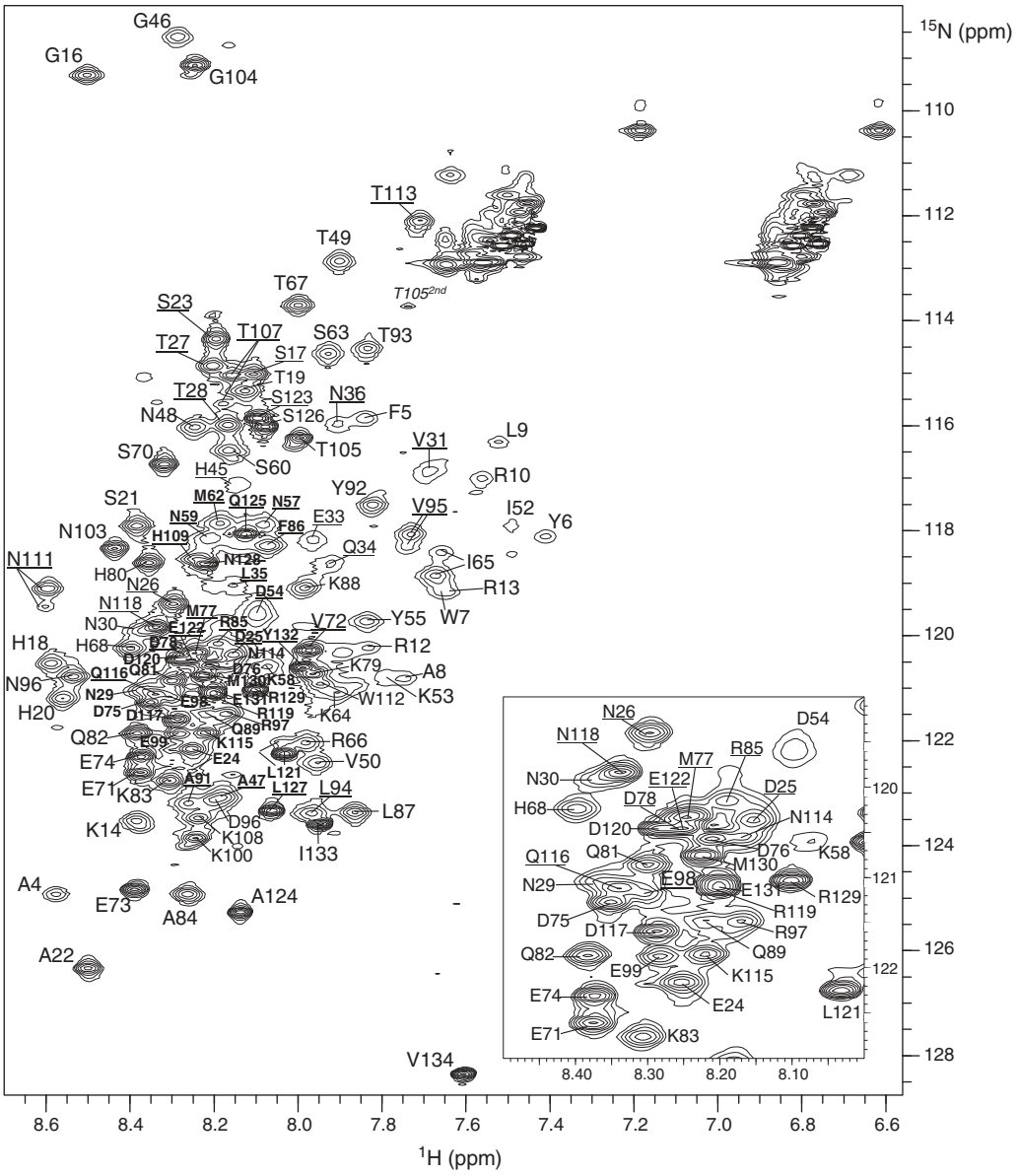

Fig. 3. NMR. ^{1}H–^{15}N HSQC spectrum of J1_tmic (0.9 mM) in the presence of 150 mM lysophospholipid (LMPG) in 20 mM phosphate buffer, pH 6.1. For clarity, residue numbering starts with the initial methionine (M1); to obtain the actual numbering, add 1084.

include the PDZ binding motif, which display very sharp resonances. Eventually, 113 of the 125 backbone HN amides could be assigned, and 6 of the 8 prolines.

Deviations from random coil values in the Cα, C′, Hα, and Cβ chemical shifts are plotted in Fig. 4 and were used to identify secondary structure regions. Four helical segments could be mapped, h1 (T1087-R1094), h2 (T1111-N1120) and h3 (I1136-I1149) in the N-terminal half of the sequence, and h4 (R1203-R1213) in the C-terminal region preceding the PDZ binding motif. The C-terminal boundary of h2 could not be established precisely as many of the resonances in this region could not be assigned. It is thus possible that h2 extends to K1123 or even to H1129. The location of h1, h2 and h4 is in good agreement with secondary structure predictions. Helix 3 is predicted by PsiPred but not by other methods, and an additional helix is predicted between residues M1161 and R1169. Secondary shifts in this region are however very small, and not as consistent as in the other helical regions. The strong negative secondary Cα shifts observed for some residues are associated with the presence of an adjacent proline, and are not likely to indicate stretches of extended structure. The total helical content estimated from chemical shifts is ~40%, which is in good agreement with CD results taking into account that CD is very sensitive to even slight deviations from regular secondary structure, such as helix bending.

To confirm secondary structure assignments, we also acquired a 3D HNHA spectrum, from which $^{3}J_{HNH\alpha}$ were calculated (Supporting Material, Fig. S5). Because of the variations in the relaxation properties along the sequence, the accuracy of these values should be taken with care. In fact, due to the vanishing intensity of many of the HN and Hα cross peaks no quantitative information could be derived for h1, h2, and h3. For h4, an average $^{3}J_{HNH\alpha}$ of 5.6 ± 0.7 Hz was calculated over residues 120–129, which is close to the mean value of 5.7 ± 0.9 Hz obtained for all assigned residues with cross peaks of measurable intensities. Interestingly, $^{3}J_{HNH\alpha}$ values close to 8 Hz were measured for the last three residues of the PDZ binding motif, suggesting that these residues may be pre-organized in the extended conformation typical of many peptide/PDZ domain complexes.

^{15}N longitudinal (R_1) and transverse (R_2) relaxation rates were measured on the ^{15}N-J1_tmic sample in the presence of LMPG micelles (Fig. 5). R_1 relaxation rates are in the range 0.62–2.12 s^{-1}, with a mean value of 1.52 s^{-1} and a standard deviation (σ) of

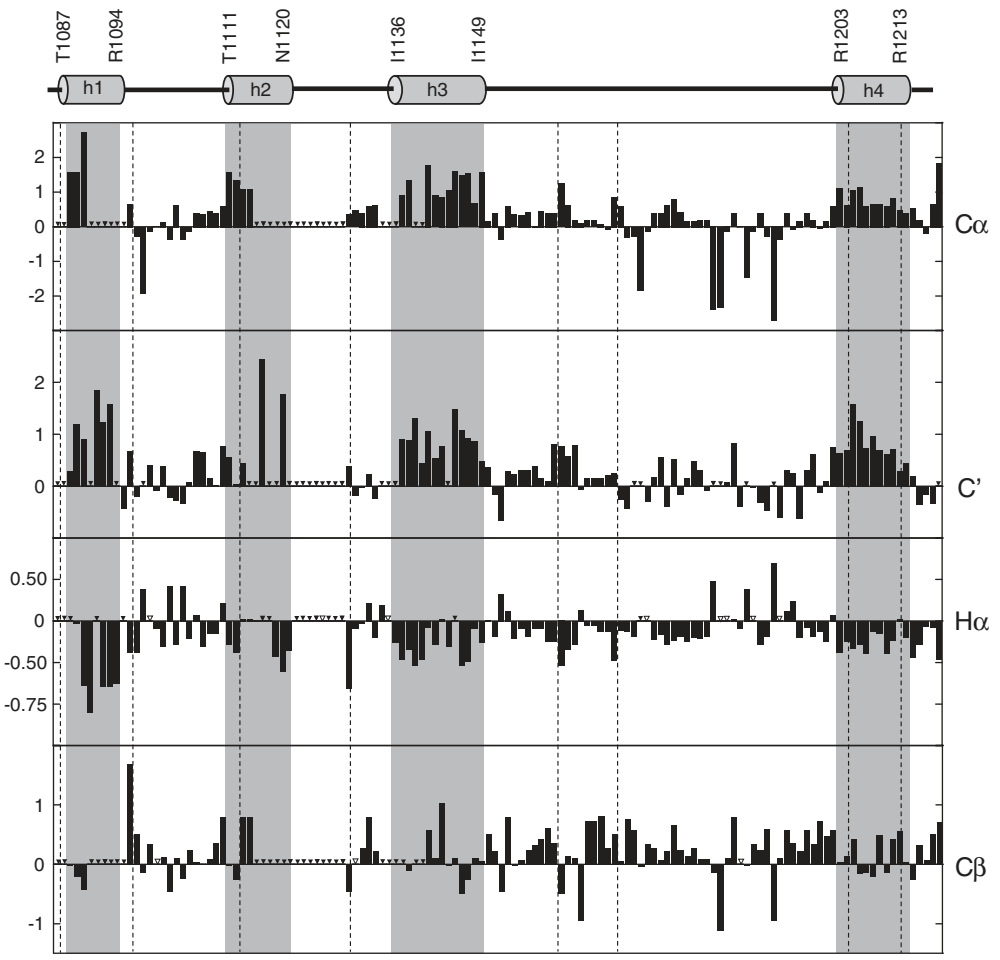

Fig. 4. Secondary structure. Deviations (ppm) of Cα, C′, Hα, and Cβ chemical shifts from random coil values and, on top, secondary structure of J1_tmic; predicted helical regions are delimited by dashed lines.

$0.27\ s^{-1}$. R_2 relaxation rates display a much wider range, varying between 2.53 and $30.6\ s^{-1}$, with a median of $10.2\ s^{-1}$ and $\sigma = 5.7\ s^{-1}$. For several peaks, R_2 values could not be determined due to vanishingly small values of the peak intensity at longer delays. The ratio R_2/R_1 was also calculated as a rough estimation of the local correlation time (τ_c) assuming isotropic motion. Values are spread between 1.4 and ~30, with a median of 6.0 and a large dispersion ($\sigma = 5.5$). There is a clear correlation between the line shape of the HN cross peaks in the ^1H–^{15}N HSQC spectrum and the R_2 values, with large R_2 values in N-terminal half of the sequence, particularly in h1, h2, and h3, and smaller R_2 values in the C-terminal half, in particular in h4 and in the PDZ binding motif, which is also displaying smaller R_1 values.

Heteronuclear ^1H–^{15}N NOEs can also provide an estimation of local backbone dynamics and are very useful in distinguishing flexible disordered regions from structured globular ones. Because of the limited dispersion in the HN chemical shifts, many regions of the HSQC spectrum suffer from severe peak overlap which, together with the very different line shapes, hamper the accurate determination of peak intensities, hence of NOE values. With these limitations in mind, a plot of ^1H–^{15}N NOEs (Fig. 5) shows a significant variability along the sequence, with a mean value of 0.37 ± 0.22. Values of ^1H–^{15}N NOEs in the N-terminal half of the sequence (mean: 0.51 ± 0.19) , in particular in the h1 (0.67 ± 0.13), h2 (0.54 ± 0.20) and h3 (0.54 ± 0.10) regions are higher than in the C-terminal half (mean: 0.27 ± 0.19). Remarkably, ^1H–^{15}N NOEs are below 0.2 in h4, with the last six residues (mean: -0.11 ± 0.28) corresponding to the PDZ binding motif displaying values that become progressively more negative.

Exchange rates of backbone HN amides with solvent were evaluated using CLEANEX experiments. Although for most of the HNs the exchange rates could not be calculated in a reliable way, a plot of the residual HN intensity in the 60 ms mixing time was helpful in identifying three regions, the loop between h1 and h2, the central portion of J1_tmic, and the C-terminal part including h4, which display relatively higher solvent exchange rates while for all isolated peaks belonging to residues h1, h2, h3 no cross peaks arising from exchange processes with the solvent were identified (Supporting Material, Fig. S6).

3.2. Effects of phosphorylation on the C-terminal region

To study the C-terminal region of Jagged-1 cytoplasmic tail in more detail, we prepared, by solid phase peptide synthesis, a peptide corresponding to the last 24 residues of Jagged-1, J1C24 (JAG1_HUMAN, residues 1195–1218), and several variants of it. To test the potential effects of phosphorylation on the intrinsic structural properties of J1C24 and on the interaction with lysophospholipid micelles, three variants were designed to include the potential phosphorylation sites adjacent to (T1197) or included in (S1207, S1210) the helical region and the potential phosphorylation site within the PDZ binding motif (Y1216). Four phosphorylated peptides were synthesized, J1C24pS, J1C24pY, J1C24pSpY, and J1C24pTpS, to cover four possible phosphorylation patterns, pS1210, pY1216,

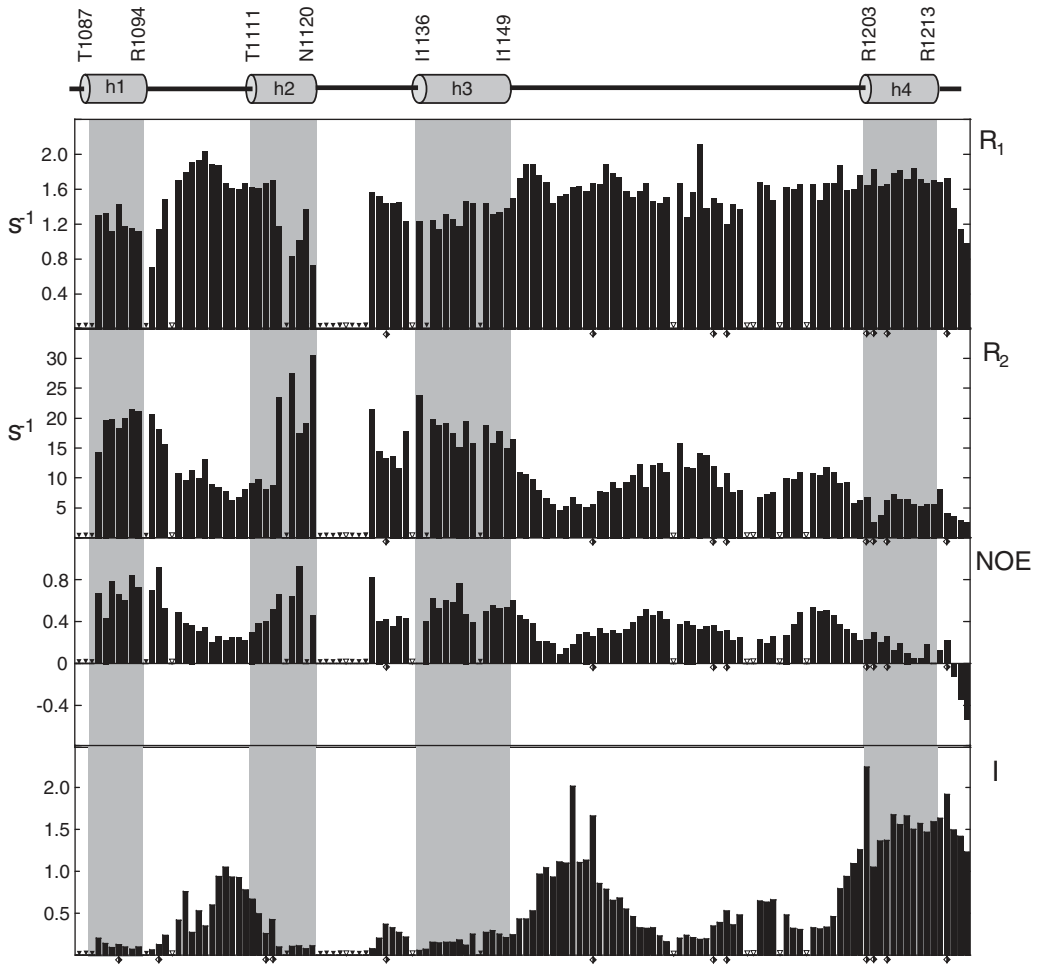

Fig. 5. Relaxation. R_1 (s^{-1}), R_2 (s^{-1}), and heteronuclear ^1H–^{15}N NOEs (I/I_{ref}) of J1_tmic; secondary structure derived from chemical shifts is drawn on top; missing HN assignments are labeled by filled triangles, prolines by empty triangles, overlapping peaks by black and white diamonds; ^1H–^{15}N HSQC peak intensities are also shown.

pS1210/pY1216, and pT1197/pS1207, respectively. An additional variant peptide, J1C24RQ, contains the R1213Q sporadic mutation found to be associated with extrahepatic biliary atresia, a congenital obstruction of the bile ducts. All peptides were designed to include (i) the C-terminal PDZ-recognition motif, (ii) the h4 helical region, (iii) W1196 for a more precise measurement of peptide concentration, and (iv) an acetylated N-terminus to avoid charge effects. Far-UV CD spectra were recorded on the peptides alone, in the presence of TFE, and in the presence of LMPC or LMPG micelles.

Far-UV CD spectra show that J1C24 is mainly disordered in buffer solution but display a significant intrinsic helical propensity in the presence of TFE and undergoes a coil–helix transition in the presence of LMPG, but not LMPC micelles (Fig. 6). The secondary structure formation is strongly pH-dependent, with an increase from 16 to 41% in the helical content in the presence of LMPG micelles when the pH is lowered from pH 7 to pH 6. Overall, CD spectra of J1C24 are consistent with CD and NMR spectra obtained for the full length J1_tmic.

The behavior of phosphorylated peptides is completely different. Phosphorylation upstream of the PDZ binding motif (pT1197, pS1207, pS1210) is sufficient to drastically reduce the intrinsic helical propensity of the peptides, as measured by far-UV CD in the presence of TFE, and to completely abolish the coil–helix transition observed for J1C24 in the presence of LMPG micelles. Phosphorylation (pY1216) or mutation (R1213Q) within the PDZ binding motif reduces the helical propensity of the peptides only partially but abolishes the conformational change observed in the presence of LMPG micelles. It can be remarked that, while J1_tmic is enriched in basic amino acids and has a quite high pI (calculated pI = 9.3), J1C24 and its variants have a negative total net charge which, taking into consideration the C-terminal carboxylate, varies from −2 for J1C24 to −6, depending on the peptide.

4. Discussion

4.1. Mimic of the membrane/cytoplasm interface

Proximal proteins and the cytoplasmic region of transmembrane proteins are peculiar, in that they “live” neither in the aqueous environment of the cytosol nor in the hydrophobic hydrocarbon core of the lipid bilayer, but rather at the interface between the two [25]. This interfacial layer is ~15 Å thick, is made by the polar groups of the fatty acid esters, the negatively charged group of the phosphate moiety, and by the phospholipid head group, which in turn determines the overall net charge of the phospholipid. The interaction of a proximal protein with the interfacial layer is mediated by charge–charge interactions, insertion of hydrophobic side chains into the hydrocarbon core, desolvation, and possibly reorganization of the lipid matrix itself. Several artificial systems have been employed to mimic the solvent/membrane interface, including SDS and DPC micelles, lysophospholipid micelles [26], bicelles [27], nanodisks [28], and large (LUV) or small (SUV or liposomes) unilamellar vesicles. All NMR experiments presented in this study were carried out with LMPG and LMPC micelles. Lysophospholipid micelles are especially attractive because they are prepared in a straightforward manner, they are relatively stable in time in the temperature and pH conditions used for acquisition of NMR data, they have a well

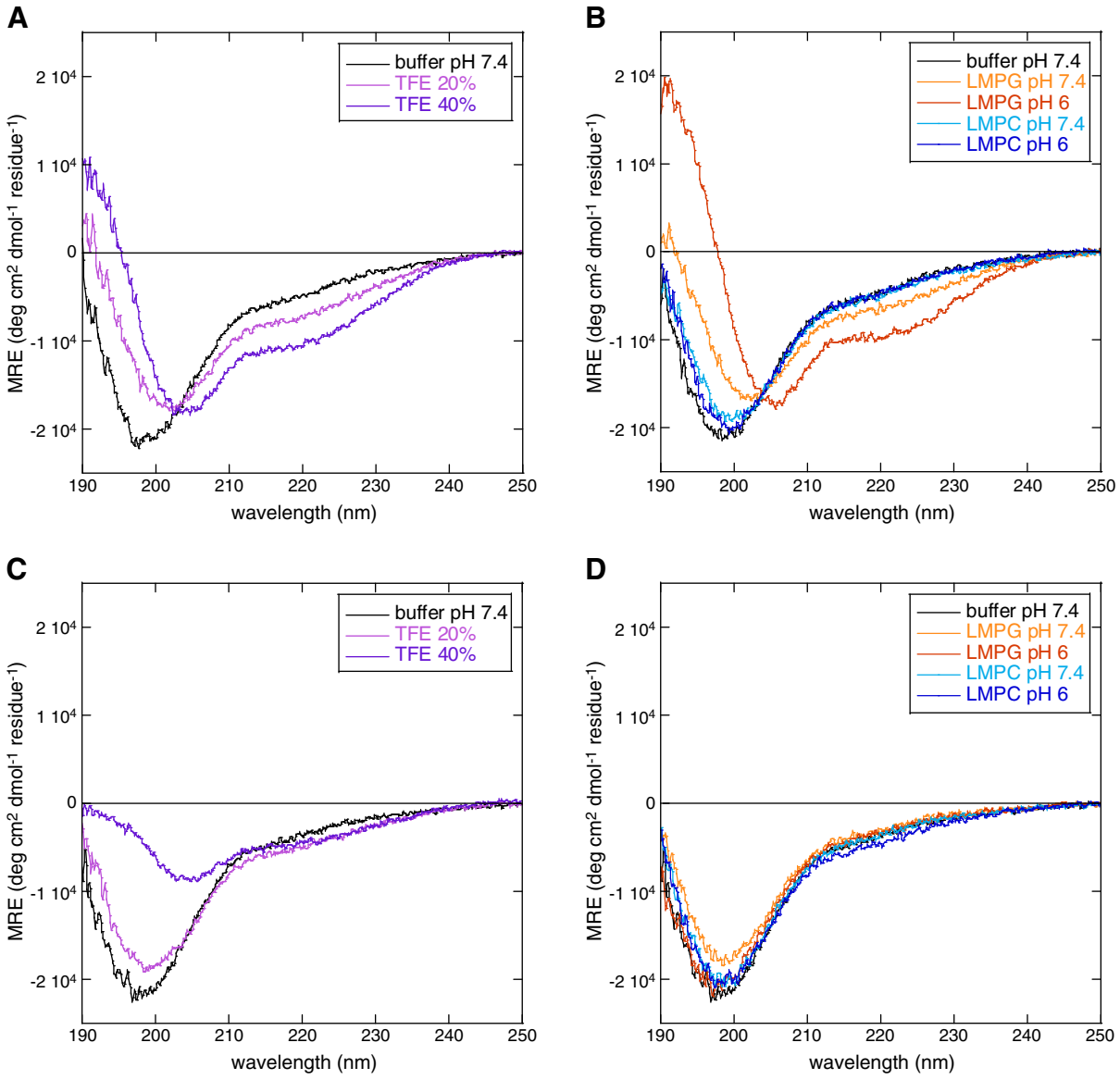

Fig. 6. Effects of phosphorylation. Far-UV CD spectra of J1C24 (A, B) and J1C24pS (C, D) in 5 mM Tris·HCl buffer and in the presence of TFE (%, v/v) or in the presence of 3 mM lysophospholipids (LMPC or LMPG) at pH 7.4 and pH 6.0. Peptide concentration was 42 μM for both J1C24 and J1C24pS.

defined composition, and they are biologically relevant, in that their head groups are identical to those found in natural phospholipids of eukaryotic plasma membranes. One of the potential drawbacks in the use of lysophospholipid micelles as models of the membrane/cytosol interface is the high curvature, which is dictated mainly by molecular size and shape. To our knowledge, structural parameters for LMPG micelles have not been yet determined precisely. A molecular mass of 35 kDa was derived by static light scattering measurements for LMPG micelles [29], which corresponds to an aggregation number of 73. This value is however significantly lower than that estimated from translational diffusion measured by NMR for LMPG-protein complexes [26] and for the related LPPG [30], LMPC [29,31], and LPPC [32] micelles, which all show aggregation numbers in the range 120–140. Small-angle X-ray scattering studies (SAXS) on LPPG micelles suggest an oblate, significantly flat disk shape rather than a spherical one, with a ratio between the two axes, a/b, of 0.65 and a gyration radius of ~37 Å [33]. Induction of secondary structure by lipid model systems in otherwise intrinsically disordered proteins has been observed in several cases, including the cytoplasmic tail of single-pass type I membrane proteins such as the ζ [34,35] and ε subunits [25] of the T cell receptor/CD3 complex. Contradictory results were however reported using different model lipid systems [36,37]. Partial folding of the T cell receptor ζ chain was induced by LMPG micelles and DMPG SUVs, but not by POPG LUVs [36,37]. It was proposed that the protein can disrupt the lipid organization of LMPG micelles and DMPG SUVs, with helix formation triggered by the interaction between the hydrocarbon tail of the lipid and the tyrosine side chains of the ITAMs (immunoreceptor tyrosine-based activation motif) [37]. In more stable systems such as POPG LUVs, the organization of the lipid bilayer would be maintained and the interaction restricted to the interface, with no folding observed upon binding. Given that curvature effects are hardly predictable, and that we observed a consistent behavior of J1_tmic going from SDS micelles to LMPG or LMPC micelles, and to DMPG or DMPC liposomes, we reasoned that lysophospholipid micelles may represent a good model system at this stage. We have no evidence, so far, of hydrophobic interactions occurring between J1_tmic and the hydrocarbon portion of the micelles as the driving force for the observed conformational changes. As already discussed [15], the consistent behavior of J1_tmic in relation to the charge of the micelle surface, rather than its lipid composition, the pH dependence of the conformational change, and tryptophan

fluorescence spectroscopy (data not shown) all point toward the interaction between J1_tmic and the interfacial layer of the micelle.

4.2. A model of Jagged-1 cytoplasmic tail at the membrane/cytoplasm interface

The lack of chemical shift dispersion in the backbone amide ^{1}H chemical shifts of J1_tmic in buffer is consistent with a mainly disordered state of the protein in solution and in agreement with previous studies [15]. In the presence of LMPC micelles, the appearance of a few new peaks and the doubling of W side chain $^{\varepsilon 1}$NH resonances suggest that, although remaining mainly unstructured, J1_tmic could interact, through the hydrophobic residues in its N-terminal region, with the hydrophobic core of the lysophospholipid micelle. This interaction is likely to be local, as most of the other resonances are not affected. This is consistent with the results obtained by circular dichroism (CD) where little or no difference was detected between the far-UV CD spectrum of J1_tmic in buffer and that of the protein in the presence of LMPC micelles [15]. On the contrary, the differences observed in the HSQC spectrum of J1_tmic in the presence of LMPG micelles show that a significant interaction is occurring between the protein and the micelle. These differences are in agreement with far-UV CD spectra, which show a coil–helix transition of J1_tmic in the presence of LMPG micelles [15]. For technical reasons, we were not able to accurately measure the affinity constants of J1_tmic for LMPG and LMPC micelles by SPR. In support of CD and NMR results, K_d values measured by SPR for J1_tmic binding to DMPG liposomes, which bear the same head groups as LMPG, were in the micromolar range, while there was no binding to DMPC liposomes. Whereas LMPC is zwitterionic, with the external layer of the micelle dominated by the positive charge of the choline moiety, LMPG is negatively charged because of the phosphate moiety. It is thus possible that the interaction between J1_tmic, which has a calculated pI of 9.3, a total of 29 positively charged residues (R + K + H) and a net charge of +10, and the negatively charged LMPG micelle is favored by electrostatic interactions. Indeed, we initially proposed [15] that the increase in the helical content of J1_tmic observed when the pH is decreased from 7 to 6 in the presence of negatively charged SDS micelles or DMPG liposomes and confirmed here may be due to the protonation of the six endogenous histidines. Results obtained for J1C24 do not support however this hypothesis. Although both J1_tmic and J1C24 show a very similar pH-dependence in their conformational change, the J1C24 sequence does not contain any histidine. This suggests that protonation of other residues, most likely aspartate and glutamate side chains, as well as the carboxylate group at the C-terminus might be involved. Desolvation at the interface between the protein and the phospholipids could destabilize the carboxylate group in favor of its protonated form. Coordination of calcium ions could reduce or neutralize the negative charge of E/D residues. Charge–charge interactions, although important, are not likely to be the only driving force for binding. The small but measurable shifts in the positions of the W side chain $^{\varepsilon 1}$NHs might be indicative of the insertion of J1_tmic hydrophobic N-terminal residues in the lipid core of the micelle. The fairly good chemical shift dispersion in the N/Q side chain NHs suggests a difference in the environment experienced and possibly specific hydrogen bonding. Even more interestingly, the appearance of relatively sharp, distinct resonances that can be tentatively assigned to $^{\varepsilon}$NHs of the R side chain suggests the presence of hydrogen bonds between these atoms and possibly the negatively charged phosphate groups of the LMPG micelle.

A short segment of basic amino acids is present in the intracellular region of most type I membrane proteins, close to the transmembrane region. Lipid binding of the intracellular region of several multichain immune receptors was shown to be related to the presence of clusters of basic residues [36]. Targeting of proteins to the membrane through basic segments occurring in mainly disordered regions has been shown for src [38], K-ras4B [39], rac1 [40] and PLC-ζ [41]. Recombinant fluorescent probes exploiting electrostatic interactions with the plasma membrane have been used to study the changes in charge distribution occurring during phagocytosis [42]. On the other hand, basic amino acids are also found in nuclear localization signals [43]. For Jagged-1, which undergoes regulated intramembrane proteolysis, basic segments may thus play a dual role, stabilizing the interaction with the inner leaflet of the plasma membrane and targeting the intracellular region to the nucleus, once the cytoplasmic tail has been proteolytically cleaved.

Backbone resonance assignments, mapping of the secondary structure, together with relaxation and solvent exchange studies, lead to a schematic model of J1_tmic bound to LMPG micelles (Fig. 7). The wide variability of R_2 values can be due very different local correlation times, to strong anisotropy, and to exchange processes and, given the complexity of this molecular system, all these mechanisms can contribute at the same time. A possible scenario consistent with the observed line widths, relaxation and solvent exchange data is given by the presence of regions that are partially or totally embedded in the micelle (h1, h2, and h3), regions that bind the surface of the micelle, probably in a dynamical way (h4), and other regions that do not significantly interact with the micelle and freely tumble in solution (the C-terminal PDZ binding motif).

4.3. Phosphorylation as a modulator of protein–protein interactions at the membrane/cytoplasm interface

If electrostatic interactions between the basic intracellular region of Jagged-1 and the negatively charged phospholipids of the membrane are important, it can be expected that phosphorylation, which is reducing the positive net charge, might significantly reduce the

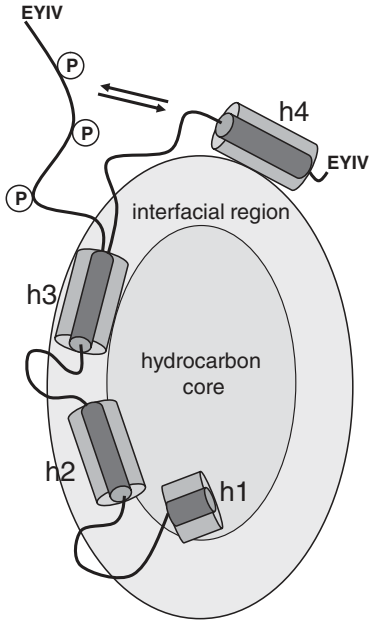

Fig. 7. Model of J1_tmic bound to micelles. The micelle is drawn as an ellipsoid with an internal hydrocarbon region and an external interfacial region. In J1_tmic, helices are drawn as cylinders with an internal (dark gray) and an external (light gray) region representing the approximate volume occupied by the backbone and the side chains, respectively. The diameter of a helix roughly corresponds to the thickness of the interfacial layer (~15 Å). In this model, h1 interacts with the hydrocarbon core of the micelle, h2 and h3 are embedded, to a different extent, in the interfacial layer, whereas h4 is floating on the surface of the micelle. Potential phosphorylation sites are indicated by a circled P.

affinity of J1_tmic for the membrane. In fact, all the C-terminal J1C24 peptides used have a negative total charge, ranging from −2 to −6 (including the C-terminus) depending on the phosphorylation state of peptide. The interaction of J1C24 with negatively charged LMPG micelles is then more likely to be due to conformation dependent insertion of hydrophobic side chains into the lipid core, specific charge interactions and possibly to hydrogen bonding. Of the several phosphorylation sites predicted in the intracellular region of Jagged-1, experimental evidence of phosphorylation in murine or human cell lines was found for Y1139 [44,45], Y1176 [45,46], and S1210 [45]. We showed that phosphorylation of residues upstream to the PDZ binding motif does not significantly affect the affinity for the afadin PDZ domain [22]. Here, we show that phosphorylation of residues upstream to the PDZ binding motif (including S1210) does have an effect on the conformation and binding of Jagged-1 C-terminal region to model membranes. Phosphorylation of residues within the PDZ recognition sequences has been shown to change the affinity for the target PDZ domains. It can be speculated that phosphorylation of residues upstream of the PDZ binding motif provides an additional mechanism to modulate the interaction of Jagged-1 cytoplasmic tail with its target PDZ containing protein, decreasing the affinity for the membrane and increasing the accessibility of the PDZ-binding motif. A recent study [47] showed that the interaction between the positively charged cytoplasmic tail of stargazin, a membrane protein associated with synaptic ionotropic glutamate receptors (AMPA), and its target PDZ domain from PSD-95 is activated by stargazin phosphorylation and its dissociation from the membrane. This mechanism is thus likely to be quite general, and may control the interaction between interfacial proteins and different protein domains through the modulation of the accessibility of the binding motif.

5. Conclusions

The cytoplasmic tail of transmembrane ligands and receptors play a functionally important role as final effectors in signal transduction from the extra- to the intracellular environment. Nevertheless, very few of these systems have been studied, partly because of the complexity of the physical milieu of residence, the interface between the plasma membrane and the cytosol. Here, we propose a model of the cytoplasmic tail of the Notch ligand Jagged-1 based on NMR and CD studies carried out on an artificial system comprising a recombinant protein, J1_tmic, and negatively charged lysophospholipid micelles used to mimic the interfacial region of the membrane. In our model, four different helical segments mediate the interaction of Jagged-1 with the membrane, while the C-terminal region that bears the PDZ interaction motif remains highly flexible. We also propose that phosphorylation of specific residues upstream of the PDZ binding motif, abolishing the intrinsic helical propensity of that region, also changes its affinity for the membrane thus contributing, in an indirect way, to the interaction with the target protein.

Acknowledgements

We are strongly indebted to Dr. Doriano Lamba (CNR-ELETTRA, Trieste, Italy) for the extensive use of the CD spectropolarimeter and to Corrado Guarnaccia (ICGEB, Protein Structure and Bioinformatics Group) for his continuous technical help. We acknowledge the Bio-NMR project (number 261863) funded by the 7th Framework Programme of the EC for financial support and access to NMR facilities.

Appendix A. Supplementary data

Supplementary data to this article can be found online at doi:10.1016/j.bbamem.2012.03.012.

References

[1] B. D'Souza, A. Miyamoto, G. Weinmaster, The many facets of Notch ligands, Oncogene 27 (2008) 5148–5167.
[2] Y. Xue, X. Gao, C.E. Lindsell, C.R. Norton, B. Chang, C. Hicks, M. Gendron-Maguire, E.B. Rand, G. Weinmaster, T. Gridley, Embryonic lethality and vascular defects in mice lacking the Notch ligand Jagged1, Hum. Mol. Genet. 8 (1999) 723–730.
[3] M. Hrabe de Angelis, J. McIntyre II, A. Gossler, Maintenance of somite borders in mice requires the Delta homologue DII1, Nature 386 (1997) 717–721.
[4] N.W. Gale, M.G. Dominguez, I. Noguera, L. Pan, V. Hughes, D.M. Valenzuela, A.J. Murphy, N.C. Adams, H.C. Lin, J. Holash, G. Thurston, G.D. Yancopoulos, Haploinsufficiency of delta-like 4 ligand results in embryonic lethality due to major defects in arterial and vascular development, Proc. Natl. Acad. Sci. U. S. A. 101 (2004) 15949–15954.
[5] R. Jiang, Y. Lan, H.D. Chapman, C. Shawber, C.R. Norton, D.V. Serreze, G. Weinmaster, T. Gridley, Defects in limb, craniofacial, and thymic development in Jagged2 mutant mice, Genes Dev. 12 (1998) 1046–1057.
[6] A. Pintar, A. De Biasio, M. Popovic, N. Ivanova, S. Pongor, The intracellular region of Notch ligands: does the tail make the difference? Biol. Direct 2 (2007) 19.
[7] J.M. Ascano, L.J. Beverly, A.J. Capobianco, The C-terminal PDZ-ligand of JAGGED1 is essential for cellular transformation, J. Biol. Chem. 278 (2003) 8771–8779.
[8] B. Hock, B. Bohme, T. Karn, T. Yamamoto, K. Kaibuchi, U. Holtrich, S. Holland, T. Pawson, H. Rubsamen-Waigmann, K. Strebhardt, PDZ-domain-mediated interaction of the Eph-related receptor tyrosine kinase EphB3 and the ras-binding protein AF6 depends on the kinase activity of the receptor, Proc. Natl. Acad. Sci. U. S. A. 95 (1998) 9779–9784.
[9] B.K. Koo, H.S. Lim, R. Song, M.J. Yoon, K.J. Yoon, J.S. Moon, Y.W. Kim, M.C. Kwon, K.W. Yoo, M.P. Kong, J. Lee, A.B. Chitnis, C.H. Kim, Y.Y. Kong, Mind bomb 1 is essential for generating functional Notch ligands to activate Notch, Development 132 (2005) 3459–3470.
[10] B.K. Koo, M.J. Yoon, K.J. Yoon, S.K. Im, Y.Y. Kim, C.H. Kim, P.G. Suh, Y.N. Jan, Y.Y. Kong, An obligatory role of mind bomb-1 in notch signaling of mammalian development, PLoS One 2 (2007) e1221.
[11] M. Yamamoto, R. Morita, T. Mizoguchi, H. Matsuo, M. Isoda, T. Ishitani, A.B. Chitnis, K. Matsumoto, J.G. Crump, K. Hozumi, S. Yonemura, K. Kawakami, M. Itoh, Mib-Jag1-Notch signalling regulates patterning and structural roles of the notochord by controlling cell-fate decisions, Development 137 (2010) 2527–2537.
[12] E. Koutelou, S. Sato, C. Tomomori-Sato, L. Florens, S.K. Swanson, M.P. Washburn, M. Kokkinaki, R.C. Conaway, J.W. Conaway, N.K. Moschonas, Neuralized-like 1 (Neurl1) targeted to the plasma membrane by N-myristoylation regulates the Notch ligand Jagged1, J. Biol. Chem. 283 (2008) 3846–3853.
[13] M.J. LaVoie, D.J. Selkoe, The Notch ligands, Jagged and Delta, are sequentially processed by alpha-secretase and presenilin/gamma-secretase and release signaling fragments, J. Biol. Chem. 278 (2003) 34427–34437.
[14] C.A. Parr-Sturgess, D.J. Rushton, E.T. Parkin, Ectodomain shedding of the Notch ligand Jagged1 is mediated by ADAM17, but is not a lipid-raft-associated event, Biochem. J. 432 (2010) 283–294.
[15] M. Popovic, A. De Biasio, A. Pintar, S. Pongor, The intracellular region of the Notch ligand Jagged-1 gains partial structure upon binding to synthetic membranes, FEBS J. 274 (2007) 5325–5336.
[16] W. Bermel, I. Bertini, I.C. Felli, R. Pierattelli, Speeding up (13)C direct detection biomolecular NMR spectroscopy, J. Am. Chem. Soc. 131 (2009) 15339–15345.
[17] W. Bermel, I. Bertini, V. Csizmok, I.C. Felli, R. Pierattelli, P. Tompa, H-start for exclusively heteronuclear NMR spectroscopy: the case of intrinsically disordered proteins, J. Magn. Reson. 198 (2009) 275–281.
[18] W. Bermel, I. Bertini, I.C. Felli, M. Piccioli, R. Pierattelli, ^{13}C-detected protonless NMR spectroscopy of proteins in solution, Prog. Nucl. Magn. Reson. Spectrosc. 48 (2006) 25–45.
[19] G.W. Vuister, A. Bax, Quantitative J correlation: a new approach for measuring homonuclear three-bond $J_{HNH\alpha}$ coupling constants in ^{15}N-enriched proteins, J. Am. Chem. Soc. 115 (1993) 7772–7777.
[20] T.L. Hwang, P.C. van Zijl, S. Mori, Accurate quantitation of water-amide proton exchange rates using the phase-modulated CLEAN chemical EXchange (CLEANEX-PM) approach with a Fast-HSQC (FHSQC) detection scheme, J. Biomol. NMR 11 (1998) 221–226.
[21] Y. Wang, O. Jardetzky, Probability-based protein secondary structure identification using combined NMR chemical-shift data, Protein Sci. 11 (2002) 852–861.
[22] M. Popovic, J. Bella, V. Zlatev, V. Hodnik, G. Anderluh, P.N. Barlow, A. Pintar, S. Pongor, The interaction of Jagged-1 cytoplasmic tail with afadin PDZ domain is local, folding-independent, and tuned by phosphorylation, J. Mol. Recognit. 24 (2011) 245–253.
[23] M. Besenicar, P. Macek, J.H. Lakey, G. Anderluh, Surface plasmon resonance in protein–membrane interactions, Chem. Phys. Lipids 141 (2006) 169–178.
[24] G. Anderluh, M. Besenicar, A. Kladnik, J.H. Lakey, P. Macek, Properties of nonfused liposomes immobilized on an L1 Biacore chip and their permeabilization by a eukaryotic pore-forming toxin, Anal. Biochem. 344 (2005) 43–52.
[25] C. Xu, E. Gagnon, M.E. Call, J.R. Schnell, C.D. Schwieters, C.V. Carman, J.J. Chou, K.W. Wucherpfennig, Regulation of T cell receptor activation by dynamic membrane binding of the CD3epsilon cytoplasmic tyrosine-based motif, Cell 135 (2008) 702–713.
[26] R.D. Krueger-Koplin, P.L. Sorgen, S.T. Krueger-Koplin, I.O. Rivera-Torres, S.M. Cahill, D.B. Hicks, L. Grinius, T.A. Krulwich, M.E. Girvin, An evaluation of detergents for NMR structural studies of membrane proteins, J. Biomol. NMR 28 (2004) 43–57.

[27] R.S. Prosser, F. Evanics, J.L. Kitevski, M.S. Al-Abdul-Wahid, Current applications of bicelles in NMR studies of membrane-associated amphiphiles and proteins, Biochemistry 45 (2006) 8453–8465.
[28] J. Borch, T. Hamann, The nanodisc: a novel tool for membrane protein studies, Biol. Chem. 390 (2009) 805–814.
[29] J. Benach, Y.T. Chou, J.J. Fak, A. Itkin, D.D. Nicolae, P.C. Smith, G. Wittrock, D.L. Floyd, C.M. Golsaz, L.M. Gierasch, J.F. Hunt, Phospholipid-induced monomerization and signal-peptide-induced oligomerization of SecA, J. Biol. Chem. 278 (2003) 3628–3638.
[30] J.J. Chou, J.L. Baber, A. Bax, Characterization of phospholipid mixed micelles by translational diffusion, J. Biomol. NMR 29 (2004) 299–308.
[31] M. Peric, M. Alves, B.L. Bales, Combining precision spin-probe partitioning with time-resolved fluorescence quenching to study micelles. Application to micelles of pure lysomyristoylphosphatidylcholine (LMPC) and LMPC mixed with sodium dodecyl sulfate, Chem. Phys. Lipids 142 (2006) 1–13.
[32] H. Hayashi, T. Yamanaka, M. Miyajima, T. Imae, Aggregation numbers and shapes of lysophosphatidylcholine and lysophosphatidylethanolamine micelles, Chem. Lett. (Japan) 23 (1994) 2407.
[33] J. Lipfert, L. Columbus, V.B. Chu, S.A. Lesley, S. Doniach, Size and shape of detergent micelles determined by small-angle X-ray scattering, J. Phys. Chem. B 111 (2007) 12427–12438.
[34] D. Aivazian, L.J. Stern, Phosphorylation of T cell receptor zeta is regulated by a lipid dependent folding transition, Nat. Struct. Biol. 7 (2000) 1023–1026.
[35] E. Duchardt, A.B. Sigalov, D. Aivazian, L.J. Stern, H. Schwalbe, Structure induction of the T-cell receptor zeta-chain upon lipid binding investigated by NMR spectroscopy, Chembiochem 8 (2007) 820–827.
[36] A.B. Sigalov, D.A. Aivazian, V.N. Uversky, L.J. Stern, Lipid-binding activity of intrinsically unstructured cytoplasmic domains of multichain immune recognition receptor signaling subunits, Biochemistry 45 (2006) 15731–15739.
[37] A.B. Sigalov, G.M. Hendricks, Membrane binding mode of intrinsically disordered cytoplasmic domains of T cell receptor signaling subunits depends on lipid composition, Biochem. Biophys. Res. Commun. 389 (2009) 388–393.
[38] D. Murray, L. Hermida-Matsumoto, C.A. Buser, J. Tsang, C.T. Sigal, N. Ben-Tal, B. Honig, M.D. Resh, S. McLaughlin, Electrostatics and the membrane association of Src: theory and experiment, Biochemistry 37 (1998) 2145–2159.
[39] J.F. Hancock, K. Cadwallader, H. Paterson, C.J. Marshall, A CAAX or a CAAL motif and a second signal are sufficient for plasma membrane targeting of ras proteins, EMBO J. 10 (1991) 4033–4039.
[40] D. Michaelson, J. Silletti, G. Murphy, P. D'Eustachio, M. Rush, M.R. Philips, Differential localization of Rho GTPases in live cells: regulation by hypervariable regions and RhoGDI binding, J. Cell Biol. 152 (2001) 111–126.
[41] M. Nomikos, A. Mulgrew-Nesbitt, P. Pallavi, G. Mihalyne, I. Zaitseva, K. Swann, F.A. Lai, D. Murray, S. McLaughlin, Binding of phosphoinositide-specific phospholipase C-zeta (PLC-zeta) to phospholipid membranes: potential role of an unstructured cluster of basic residues, J. Biol. Chem. 282 (2007) 16644–16653.
[42] T. Yeung, M. Terebiznik, L. Yu, J. Silvius, W.M. Abidi, M. Philips, T. Levine, A. Kapus, S. Grinstein, Receptor activation alters inner surface potential during phagocytosis, Science 313 (2006) 347–351.
[43] A. Lange, R.E. Mills, C.J. Lange, M. Stewart, S.E. Devine, A.H. Corbett, Classical nuclear localization signals: definition, function, and interaction with importin alpha, J. Biol. Chem. 282 (2007) 5101–5105.
[44] A. Guo, J. Villen, J. Kornhauser, K.A. Lee, M.P. Stokes, K. Rikova, A. Possemato, J. Nardone, G. Innocenti, R. Wetzel, Y. Wang, J. MacNeill, J. Mitchell, S.P. Gygi, J. Rush, R.D. Polakiewicz, M.J. Comb, Signaling networks assembled by oncogenic EGFR and c-Met, Proc. Natl. Acad. Sc.i U. S. A. 105 (2008) 692–697.
[45] C. Pan, F. Gnad, J.V. Olsen, M. Mann, Quantitative phosphoproteome analysis of a mouse liver cell line reveals specificity of phosphatase inhibitors, Proteomics 8 (2008) 4534–4546.
[46] A. Moritz, Y. Li, A. Guo, J. Villen, Y. Wang, J. MacNeill, J. Kornhauser, K. Sprott, J. Zhou, A. Possemato, J.M. Ren, P. Hornbeck, L.C. Cantley, S.P. Gygi, J. Rush, M.J. Comb, Akt-RSK-S6 kinase signaling networks activated by oncogenic receptor tyrosine kinases, Sci. Signal. 3 (2010) ra64.
[47] A. Sumioka, D. Yan, S. Tomita, TARP phosphorylation regulates synaptic AMPA receptors through lipid bilayers, Neuron 66 (2010) 755–767.